Photophysical Properties of Sulfone-Based TADF Emitters In Relation To Their Structural Properties

Aslıhan Hepguler,[‡] Pelin Ulukan[‡] and Saron Catak*

Bogazici University, Department of Chemistry, Bebek, 34342, Istanbul, Turkey

ABSTRACT

In this work, Thermally Activated Delayed Fluorescence (TADF) of a series of emitters with sulfone-based acceptor moieties were studied by Density Functional Theory (DFT) methods. Sulfone derivatives were shown to be high performing TADF emitters over recent years. When discussing the TADF efficiency, various properties, such as, singlet–triplet energy gap (ΔE_{ST}), spin–orbit coupling (SOC), nature of states and the hyperfine coupling (HF) stand out due to their roles in reverse intersystem crossing (RISC). Here, we mainly focused on three important structural parameters that affect the intersystem crossing (ISC) and RISC pathways and their efficiencies. These three parameters are: 1) effect of *meta*- and *para*-conjugation, 2) effect of rigid acceptor moieties and 3) effect of phenyl bridge on photophysical properties.

INTRODUCTION

In recent years, Thermally Activated Delayed Fluorescence (TADF) materials have attracted considerable attention due to their 100 % exciton harvesting abilities and high device efficiencies.[1] For traditional fluorescent materials, known as organic light emitting diodes (OLEDs), only 25 % of excitons lead to luminescence, and the remaining 75 % are triplets that are deactivated by nonradiative transitions.[2–4] To overcome low device efficiencies of fluorescent emitters, phosphorescent materials (PhOLEDs) containing heavy metals were developed and due to their emission from triplet state to ground state, the loss of triplet excitons was prevented.[5,6] Although the loss of excitons were prevented, the heavy metals in their structure led to undesirable consequences, such as, high cost and environmental pollution.[7] In 2012, Adachi and co-workers developed TADF materials as a promising technology, which provides high efficiency, cost saving and environmentally friendly applications (Figure 1).[2,8–10] Due to the efficient harvesting of triplet excitons, TADF materials offer advanced applications in electroluminescence,[11] sensors,[12] bioimaging,[10,12] and organic lasers.[13]

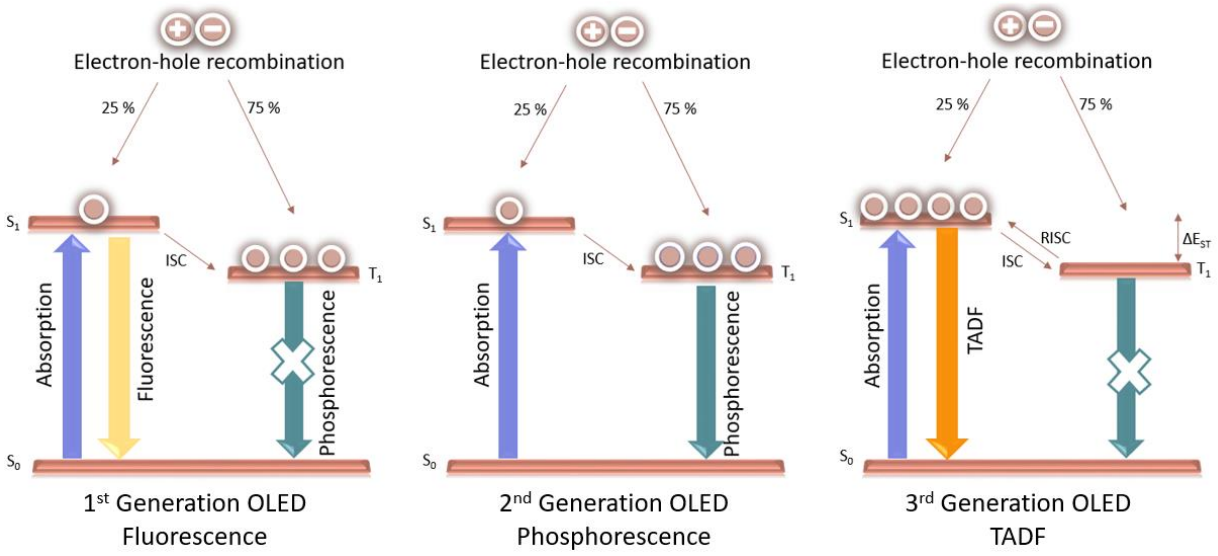

Figure 1. OLED, PhOLED and TADF mechanism.

Metal free TADF emitters can achieve 100 % internal quantum efficiencies by harvesting triplet excitons *via* the RISC process from the first excited triplet state (T_1) to the first excited singlet state (S_1) under thermal activation.[14–17] Many TADF materials usually adopt a twisted donor (D)–acceptor (A) geometry to minimize the overlap between highest occupied molecular orbitals (HOMO) and lowest unoccupied molecular orbitals (LUMO), which lead to small S_1–T_1 energy gap (ΔE_{ST}).[18]

$$\Delta E_{ST} = 2 \int \int \Phi_L(1)\Phi_H(2) \frac{e^2}{r_1 - r_2} \Phi_L(2)\Phi_H(1) \mathrm{d}r_1 \mathrm{d}r_2 \quad (1)$$

As represented in the equation 1, decreasing the exchange interaction integral of the HOMO and the LUMO wavefunctions is an efficient way to minimize the ΔE_{ST}. Recent studies reported that in a cofacial configuration of D and A moieties, emitters have the possibility to exhibit Through-Space Charge-Transfer (TSCT) which leads to separation between the HOMO and LUMO, thus, leading to small ΔE_{ST} values. However, compared to the Through-Bond Charge-Transfer (TBCT) systems, TSCT systems have relatively lower electronic interactions between D and A moieties, which lead to increased rotations between D and A groups and strong non-radiative decays.[19] To sum up, there are two possible ways of separating frontier molecular orbitals, which is, rationally designing TBCT and TSCT systems.

Furthermore, TADF efficiency is not only dependent on ΔE_{ST}, but also highly related to the spin–orbit coupling (SOC), that is, effective RISC relies on both small ΔE_{ST} and large SOC.[11,12,16,20,21] For many TADF emitters, due to their purely organic structures, SOCs were found to be intrinsically weak, which makes it

difficult to obtain efficient RISC in TADF and ISC in phosphorescence. To enhance SOC values in TADF emitters, the heavy–atom effect was used; since SOC is proportional to the fourth power of the nuclear charge, the most common strategy for improving SOC is introducing non-metal atoms to the molecular structure, such as halogens.[18,22]

In this work, we demonstrate photophysical and structural behaviors of a series of sulfone-based TADF emitters using computational methods. As listed in Figure 2, the set of molecules under investigation has various sulfone-based acceptor moieties such as; diphenylsulfone (DPS), dibenzo- thiophene-S, S,-dioxide (DBTO2), 9,9-dimethyl-9H-thioxanthene 10,10-dioxide (TXO2), and thianthrene 5,5,10,10-tetraoxide (TTR).

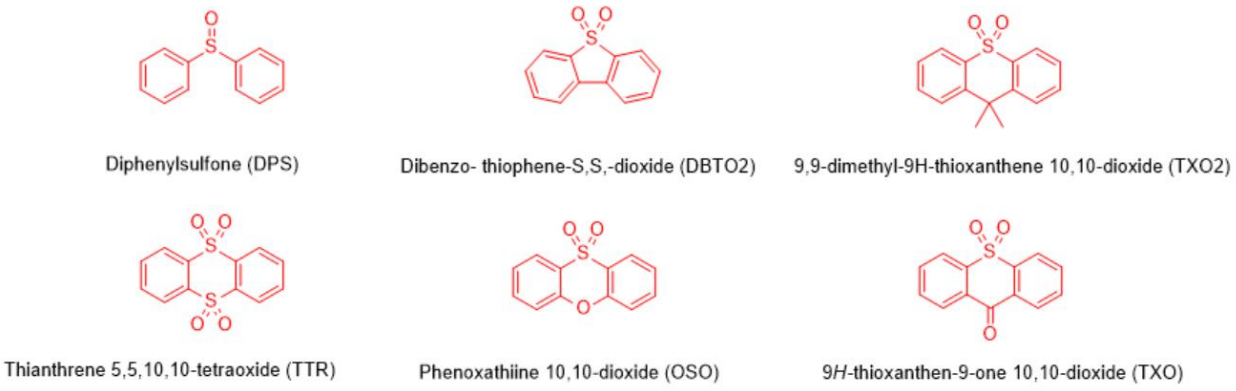

Figure 2. Sulfone based acceptor moieties investigated in this study.

The donor moieties depicted in this molecule set (Figure 2) are reported in our previous studies as well as in recent TADF literature.[7,23] In our previous reports, we theoretically investigated the characteristics of dimethylacridine (DMAC), carbazole (Cz), phenoxazine (PXZ), phenothiazine (PTZ) and diphenylamine (DPA) as donor moieties.[7] By simulating a wide molecule set with different donor and acceptor moieties, we study the effects and significance of the sulfur atom in various structures. As reported in literature, DPS is a multi-talented acceptor moiety, with strong electron withdrawing ability due to the highly electronegative oxygen atoms and provides excellent TADF activity due to its central twist.[24,25] Moreover, since it has tetrahedral geometry, it is known to restrict the π- conjugation of the emitters leading to CT compounds. While the DBTO2 and TXO2 acceptor moieties were used to understand the influence of acceptor rigidity on descriptors; the TTR group was selected to predict the effects of two iso-energetic low energy conformers $–SO_2$ unit on conjugation between D-A units and on energy levels.

THEORETICAL CALCULATIONS

To better understand the structural and photophysical properties of the emitters discussed in this study, a computational analysis was conducted using the Gaussian16[26] and Amsterdam Density Functional (ADF)[27] software packages. Geometries in the ground and excited S_1 and T_1 states were optimized at the M062X[28]/6-31+G(d,p)[29] level of theory. Tamn Dancoff Approximation (TDA)[30] calculations for the $S_0 \rightarrow S_n$ and $S_0 \rightarrow T_n$ transitions using the M062X/6-31+G(d,p) and ωB97XD[31]/6-31+G(d,p) levels were performed with respect to the optimized S_0 state geometries. This choice is due to the fact that the TDA method provides a more balanced description of both triplet and singlet excited states, and compared to Time-Dependent DFT (TD-DFT), it is free from triplet instability issues.[32] 6-311++G(3df,3pd)[33] extra basis set was used for the sulfur atom in all calculations. From the theoretical calculations, it can be observed that different acceptor and donor moieties exhibit characteristic torsions (see Tables S2-S6). Moreover, some compounds exhibit two different iso-energetic iso-energetic low energy conformers conformers presenting TADF as well as non-TADF activities. While near orthogonal geometries resulted in very small ΔE_{ST} values making the RISC process viable, planar conformers were shown to yield larger ΔE_{ST} values representing non-TADF behavior.

In order to better analyze electron processes at exited states, including internal conversion (IC), ISC and RISC processes, we report the lowest 10 states for singlet and triplet excitations. Surprisingly, energy differences between excited states show the possibility of high-energy hot exciton pathways in ISC processes. Moreover, the nature of the excited singlet and triplet states is evaluated using Natural Transition Orbitals (NTOs), obtained with the Nancy_EX code[34] and visualized with the Avogadro[35] software package. Data obtained from calculations at ωB97XD/6-31+G(d,p) level of theory were reported in Tables S7-S20.

In consideration of the first-order perturbation theory, SOC values between excited singlet and triplet geometries were computed at S_1 and T_1 geometries using the ADF software package at M062X/DZP[36] level of theory.

The ultraviolet-visible (UV-Vis) absorption spectra of the investigated emitters were modeled by generating 30 conformers through a Wigner distribution as implemented in the Newton-X software package.[37] Vertical transitions from each snapshot were convoluted using Gaussian functions of full-width at half length (FWHL) of 0.15 eV. Absorption spectra calculations via Wigner distribution method have been performed with B3LYP,[38] PBE0,[39] M062X and BLYP[38] functionals using the 6-31+G(d,p) basis set.

Integral equation formalism polarizable continuum model (IEF-PCM) was used in all calculations, to implicitly model the solvent environment.[40–42] Optimized geometries were rendered with the CYLview software package.[43]

RESULTS and DISCUSSION

Effects of *meta*- and *para*- Conjugation on Photophysical Properties

Although sulfone-based TADF emitters have been reported by several research groups, the majority of these studies focus on *para*-substituted materials. Comparatively, we theoretically investigated both *meta*- and *para*-substituted sulfone based emitters to clarify the effects of different positions of the donor moieties on photophysical properties. As depicted in Figure 3, we modeled five *meta*- and five *para*-substituted molecules with the DPS donor moiety and various donor groups, such as, Cz, PTZ, PXZ, DMAC and DPA.

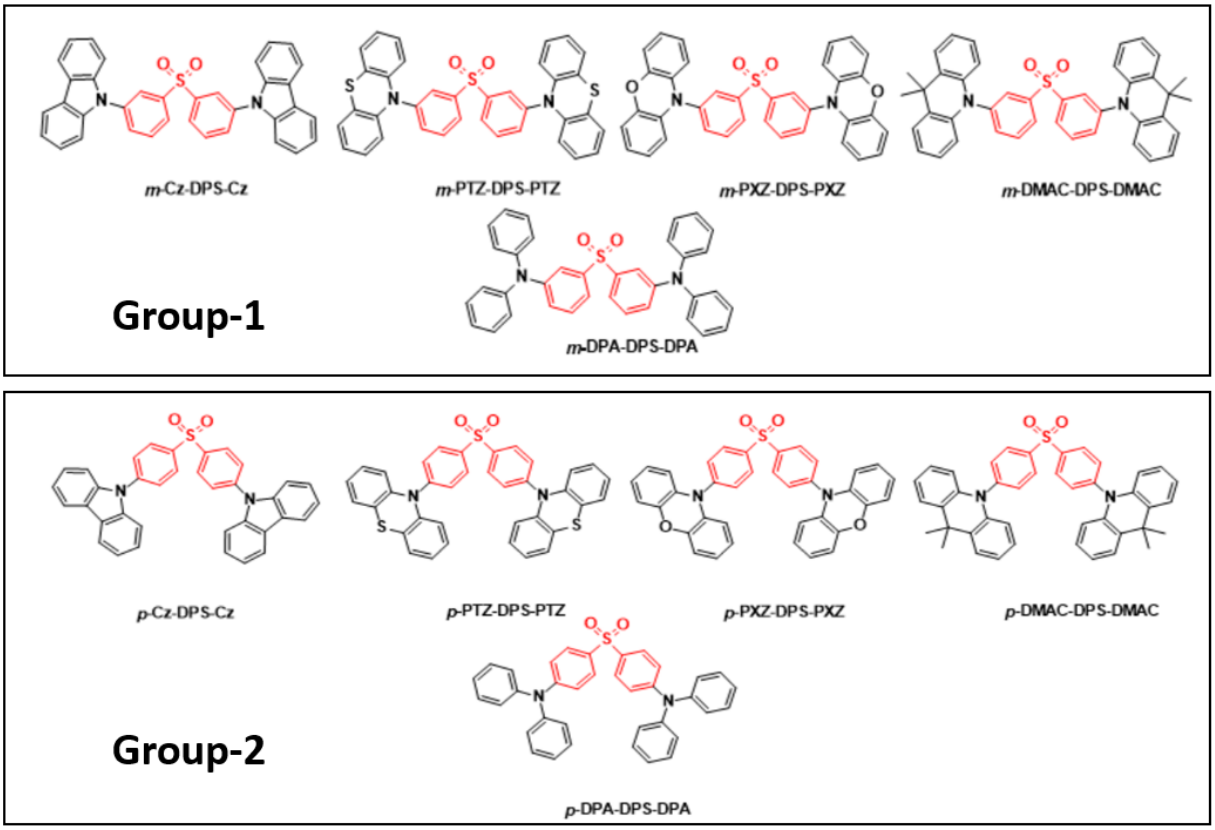

Figure 3. *Meta*- (Group 1) and *para*-substituted (Group 2) TADF emitters with DPS acceptor moiety.

Compounds: *m*-Cz-DPS-Cz,[44] *m*-PTZ-DPS-PTZ,[44] *m*-DMAC-DPS-DMAC,[44] *m*-PXZ-DPS-PXZ,[44] *m*-DPA-DPS-DPA,[44] *p*-Cz-DPS-Cz,[45] *p*-PTZ-DPS-PTZ,[46] *p*-DMAC-DPS-DMAC,[47] *p*-PXZ-DPS-PXZ,[47] *p*-DPA-DPS-DPA.[48]

It is well-known that photophysical properties of organic compounds are highly affected by geometric parameters. The majority of the studies in literature focus exclusively on symmetric emitters with D-A-D skeletons.[49] However, a few studies have been reported to clarify the effects of asymmetric emitters in TADF efficiencies .[49] Optimized geometries of *meta*- and *para*-substituted TADF emitters show that for S_0 state structures, the tetrahedral geometry of DPS moiety do not change, however, significant changes were observed in the bending of donor moieties. As reported in Tables S2 and S3, while *para*-substituted DPS containing TADF emitters yield highly symmetrical structures, their *meta*-substituted analogues have asymmetric geometries.

Herein, a comprehensive analysis on the effects of symmetric and asymmetric geometries as well as the bends in donor groups was performed. Bent conformations in ground state are known to avoid molecular aggregation and the formation of intermolecular excimers.[50] Therefore, emitters with bent donor moieties are expected to be favorable in preventing molecular aggregation, which leads to non-emissive decays.[50]

Following the geometry analyses, we further modeled the energy alignments of singlet and triplet states and aimed to investigate the differences between *meta*- and *para*-substituted emitters. Figure 4 demonstrates that except for the DPA-derivative, *para*-substituted emitters yield lower energy triplet levels compared to their *meta*- counterparts; and low-lying singlet state energies decreased in *para*-substituted emitters. Moreover, we also observed that many compounds in the first two groups exhibit iso-energetic S_1 and S_2 states, which may cause multiple emission bands with identical or different natures. On the other hand, lower energy triplet states in *para*-emitters create greater number of possible pathways for RISC process, which also leads to greater amount of exciton harvesting from iso-energetic triplet states below the S_1 level.

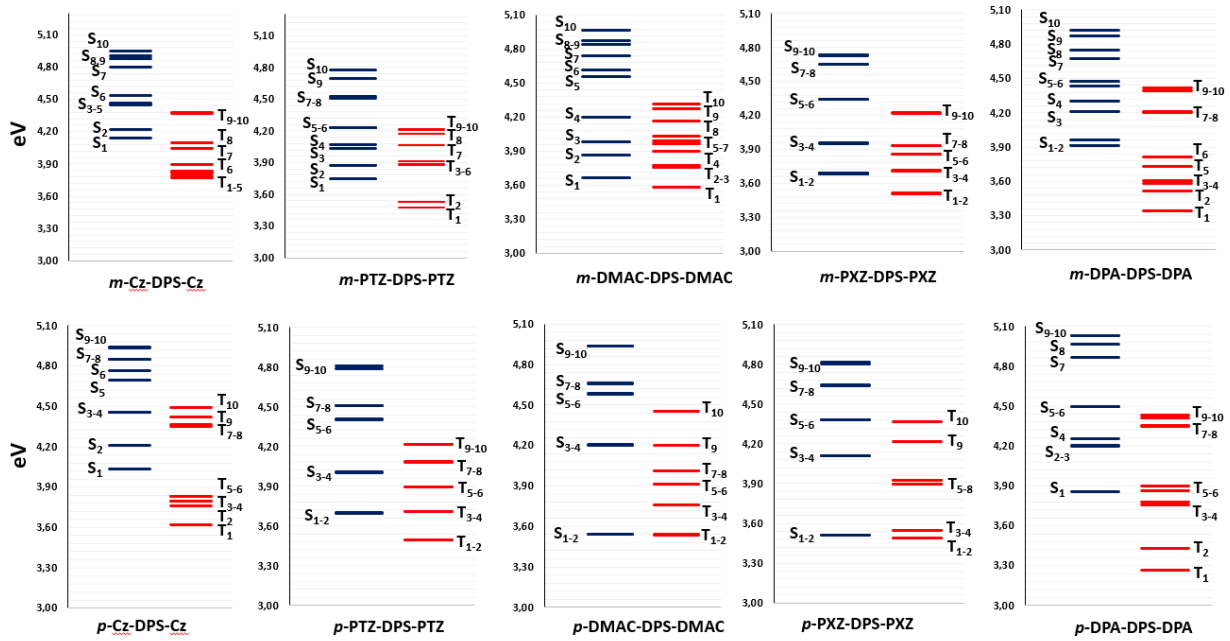

Figure 4. Energy levels of *meta*- (Group 1) and *para*-substituted (Group 2) TADF emitters computed at M062X/6-31+G(d,p) level of theory in toluene.

As shown in Figure S6, absorption spectra of *para*-substituted emitters yield lower energy bands compared to the *meta*-substituted compounds. This behavior of *para*-substitution suggests that geometries with smaller distortion cause stronger electron conjugation in the excited state. It should also be noted that theoretical absorption spectra of both *meta*- and *para*-emitters exhibit dominant high intensity bands in higher energies, indicating that while $S_0 \rightarrow S_1$ absorptions are almost negligible, strong excitations to upper singlet states are highly dominant in both Group 1 and 2 (Table S21). Comparisons between *meta*- and *para*-substituted emitters showed that *para*-substituted compounds have larger oscillator strengths, which is an important parameter in understanding excited state transitions. As listed in Table S21, except for *para*-substituted Cz-DPS-Cz and DPA-DPS-DPA emitters, compounds usually exhibit negligible transition to S_1 level and strong transitions to higher singlet states. It is also shown that for *meta*-substituted Cz-DPS-Cz emitters, absorptions with relatively larger oscillator strengths are (>0.1) S_4, S_6, S_8 and S_9. On the other hand, its *para*-substituted analogue has $S_0 \rightarrow S_1$ transition with quite strong oscillator strength, f=0.6433. Similar to the Cz-DPS-Cz emitter, *para*-substituted DPA-DPS-DPA emitter exhibits strong $S_0 \rightarrow S_1$ transition (f=0.9967), while its *meta*- analogue has negligible transition to S_1 state, and quite strong transitions to higher singlet states. For *meta*- and *para*-substituted PTZ-DPS-PTZ, PXZ-

DPS-PXZ and DMAC-DPS-DMAC emitters, strong excitations from S_0 to S_n states opens up alternative ISC channels for TADF emitters.

It is well-known that population of high energy excited states leads to more energy loss during the IC process to the S_1 level. Therefore, with the help of strong SOC values between high energy singlet and triplet states, instead of IC, emitters may experience ISC between S_n and neighboring triplet states, leading to decreased energy loss and hence, higher efficiency.[51] Population of triplet states are affected by both the energy difference and the SOC between relevant singlet and triplet states. As reported in Table S22, though strong SOC between high oscillator strength singlet states and T_1 or T_2 states is possible (such as in *meta*-Cz), a strong coupling between high-energy singlet levels and high-energy triplet levels can also be observed (such as in *meta*-PTZ). Moreover, we also observed that iso-energetic triplet states, such as, the ones observed in *m*/*p*-PXZ-DPS-PXZ, *p*-DMAC-DPS-DMAC and *p*-PTZ-DPS-PTZ compounds may exhibit SOC values in different strengths, which shows that these iso-energetic triplet levels are in different natures, ^{3}CT/^{3}LE, and state mixing processes enhancing RISC is possible in these emitters. For instance, *p*-PXZ-DPS-PXZ emitter has iso-energetic T_1 and T_2 states which have 0.64 cm^{-1} and 1.61 cm^{-1} SOC values, respectively, and this difference in SOC values can be attributed to the different natures of T_1 and T_2 states (Table 1).

Table 1. Natures of S_1, T_1-T_5 states of the emitters in Group 1 and Group 2 computed at M062X/6-31+G(d,p) level of theory in toluene.

Emitters	S_1 (Φs)	T_1 (Φs)	T_2 (Φs)	T_3 (Φs)	T_4 (Φs)	T_5 (Φs)
***m*-Cz-DPS-Cz**	CT	LE	LE	LE	LE	LE
	0.5570	0.7721	0.8095	0.8065	0.9629	0.9618
***p*-Cz-DPS-Cz**	CT-LE	CT-LE	CT-LE	LE	LE	LE
	0.7047	0.8405	0.8622	0.7503	0.7622	0.9676
***m*-PTZ-DPS- PTZ**	CT-LE	CT-LE	LE	CT-LE	CT	LE
	0.4703	0.7920	0.8164	0.5513	0.5599	0.7030
***p*-PTZ-DPS- PTZ**	CT	CT-LE	CT-LE	CT	CT	LE
	0.3310	0.7845	0.7859	0.4534	0.4614	0.6823
***m*-DMAC-DPS-DMAC**	CT	CT-LE	CT-LE	LE	LE	CT-LE
	0.3939	0.6062	0.5834	0.8424	0.7313	0.5798
***p*-DMAC-DPS-DMAC**	CT	CT	CT	LE	LE	LE
	0.1642	0.1692	0.1677	0.8800	0.8798	0.7097
***m*-PXZ-DPS-PXZ**	CT	CT-LE	CT-LE	CT-LE	CT-LE	CT-LE
	0.4383	0.7597	0.7578	0.6758	0.6576	0.5843
***p*-PXZ-DPS-PXZ**	CT	CT-LE	CT	CT-LE	CT-LE	LE
	0.2485	0.4301	0.3921	0.7840	0.7951	0.7599
***m*-DPA-DPS-DPA**	CT-LE	CT-LE	CT-LE	CT-LE	LE	LE
	0.7416	0.8193	0.7288	0.7987	0.8031	0.8448
***p*-DPA-DPS-DPA**	CT-LE	CT-LE	CT-LE	LE	LE	LE
	0.7594	0.8375	0.8465	0.8208	0.8373	0.8241

As mentioned previously, multiple triplet states below the S_1 level creates multiple RISC possibilities. To analyze the probability of RISC from different triplet levels, SOC values between relevant states were calculated. As reported in Table S22, root mean square coupling element (RMSCE, V_{SOC}), which is directly proportional to RISC rate constant have been calculated for all states (for transition between S_1 and T_1 states, $|\langle S_1|\hat{H}_{SOC}|T_1\rangle|$ is divided into three to represent the average over the three triplet states for each possible value of the total angular momentum J=−1,0,1, see the equation 3).

$$k_{RISC} = \frac{2\pi}{\hbar} \; |V_{SOC}|^2 \; x \; \rho_{FCWD} \qquad (2)$$

$$V_{SOC} = \frac{1}{3} \; |\langle S_1|\hat{H}_{SOC}|T_1\rangle| \qquad (3)$$

It is obvious that transition from any triplet state below S_1 is possible with a strong SOC value. Importantly, it was observed that the energy gaps closest to the experimental value generally exhibit strongest $|V_{SOC}|^2$, and generally, SOC values in *para*-substituted emitters are larger than the *meta*-substituted ones (except emitters Cz-DPS-Cz and PTZ-DPS-PTZ). These higher SOC values in *para*-substituted emitters can be attributed to the larger amount of state mixing in iso-energetic triplet levels below the S_1 state.

As represented in Table 2, among *meta*- and *para*-analogues, slight changes were observed in HOMO-LUMO energies and the energy difference between these two molecular orbitals (E_g). For compounds Cz-DPS-Cz, PTZ-DPS-PTZ and DMAC-DPS-DMAC, *meta*-substitution leads to larger HOMO energies, thus, stronger electron donating ability of Cz, PTZ and DMAC donor moieties. On the other hand, while the PXZ donor moiety represents almost equal HOMO energies in *meta*- and *para*-substituted emitters, their DPA analogues yield better donating ability with *para*-substitution. This behavior of DPA-DPS-DPA emitter can be attributed to the highly sterically hindered and twisted structure in *meta*-compound, which results in disruption of conjugation within the molecule. For the electron accepting ability, LUMO energies of *meta*- and *para*-substituted compounds were checked and it was observed that for PTZ-DPS-PTZ, DMAC-DPS-DMAC and PXZ-DPS-PXZ compounds, *para*-substitution leads to smaller LUMO energies and stronger electron withdrawing towards the acceptor moiety. Overall, the position of the donor moiety in these two molecule sets did not cause large differences in E_g values and these results are consistent with the similar ΔE_{ST} values of *meta*- and *para*- isomers (except Cz-DPS-Cz and PTZ-DPS-PTZ emitters).

Table 2. HOMO and LUMO energies, and energy gaps of Group 1 and Group 2 emitters computed at M062X/6-31+G(d,p) level of theory in toluene.

Emitters	HOMO	LUMO	LUMO - HOMO (E_g) (eV)	ΔE_{ST} a=experiment b=theoretical
***m*-Cz-DPS-Cz**	-0.2579	-0.0460	0.2120	0.44[a] / 0.36[b]
***p*-Cz-DPS-Cz**	-0.2594	-0.0457	0.2137	0.25-0.31[a] / 0.27[b]
***m*-PTZ-DPS- PTZ**	-0.2459	-0.0478	0.1980	0.01[a] / 0.04[b]
***p*-PTZ-DPS- PTZ**	-0.2461	-0.0488	0.1973	0.40[a] / 0.21[b]
***m*-DMAC-DPS-DMAC**	-0.2404	-0.0445	0.1959	0.05[a] / 0.09[b]
***p*-DMAC-DPS-DMAC**	-0.2421	-0.0466	0.1955	0.09[a] / 0.01[b]
***m*-PXZ-DPS-PXZ**	-0.2427	-0.0476	0.1951	0.06[a] / 0.03[b]
***p*-PXZ-DPS-PXZ**	-0.2426	-0.0499	0.1928	0.08[a] / 0.02[b]
***m*-DPA-DPS-DPA**	-0.2459	-0.0324	0.2135	- / 0.33[b]
***p*-DPA-DPS-DPA**	-0.2439	-0.0313	0.2126	0.54[a] / 0.42[b]

To further compare the RISC behaviors of *meta*- and *para*-emitters, we theoretically calculated the energy gaps between singlet and triplet states. As reported in Table 2, experimental energy gaps were well reproduced and the largest absolute deviation was obtained as 0.29 eV for *p*-PTZ-DPS-PTZ emitter. Importantly, these energy gaps correspond to the gaps between S_1 and triplet state with largest RMSCE. In particular, proving the deterministic effect of SOC is consistent with our recent study published in 2022.[23]

To summarize our findings so far, changing the position of the donor moiety from *para*- to *meta*- results in an increase in the twisting angle between donor and acceptor moieties, which is beneficial for separation of frontier molecular orbitals. For the molecules in the first two groups, we have investigated the energy level alignments of excited states. Surprisingly, there are more than one triplet states below the S_1 level. Moreover, the presented results show that there are iso-energetic singlet and triplet states, which have the possibility to contribute to ISC and RISC processes. Further analyses led us to conclude that the RISC process is mainly a SOC driven mechanism and it occurs between the states with strongest SOC values. Additionally, we also present our findings for the oscillator strength and its effect on IC/RISC pathways.

Effect of Rigidity of The Acceptor Moiety on Photophysical Properties

According to molecular design strategies, rigid compounds are good candidates for spatially separated frontier molecular orbitals, which makes them CT based compounds due to their short π–conjugation length and high steric hindrance. Therefore, here we analyzed the behaviors of rigid TXO2, DBTO acceptor moieties and flexible DPS moiety to observe and compare the photophysical differences arising from the degree of rigidity.

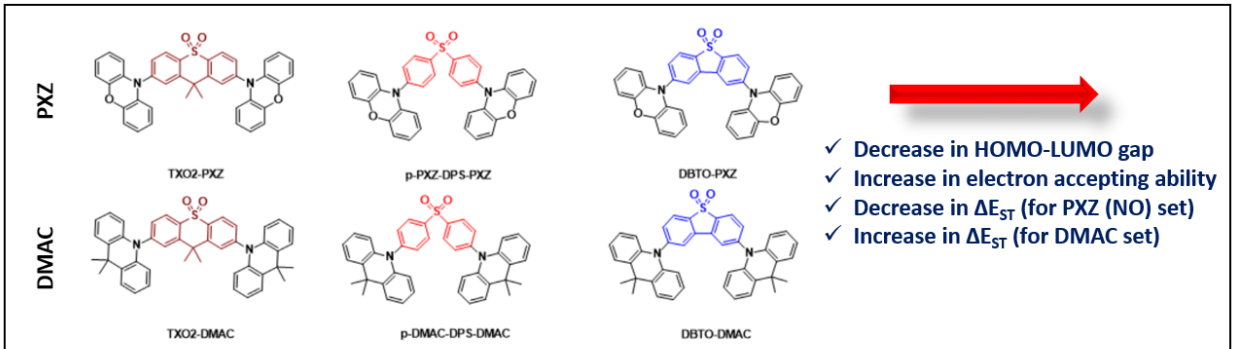

Emitters	ΔE_{ST} (eV) a=experimental b=theoretical	HOMO (eV)	LUMO (eV)	Eg (eV)	SOC	$\lvert V_{SOC}\rvert^2$	ΔΦs
TXO2-PXZ	0.040-0.010[a] 0.099[b]	-0.2417	-0.0421	0.1996	1.290	1.664	0.5563
***p*-PXZ-DPS-PXZ**	0.080[a] 0.035[b]	-0.2426	-0.0499	0.1928	0.920	0.846	0.5466
DBTO-PXZ	0.060[a] 0.035[b]	-0.2443	-0.0575	0.1867	0.870	0.167	0.1988
TXO2-DMAC	0.000[a] 0.001[b]	-0.2415	-0.0390	0.2025	1.030	1.061	0.0259
***p*-DMAC-DPS-DMAC**	0.090[a] 0.006[b]	-0.2421	-0.0466	0.1955	0.720	0.139	0.0050
DBTO-DMAC	0.090[a] 0.016[b]	-0.2428	-0.0564	0.1864	0.880	0.169	0.0390

Figure 5. Comparison of different photophysical properties for different acceptor moieties computed at M062X/6-31+G(d,p) level of theory in toluene (TXO2-PXZ, *p*-PXZ-DPS-PXZ, TXO2-DMAC, *p*-DMAC-DPS-DMAC, DBTO-DMAC) and in dichloromethane (DBTO-PXZ).
Compounds: TXO2-PXZ,[52] p-PXZ-DPS-PXZ,[53] DBTO-PXZ,[54] TXO2-DMAC,[24] p-DMAC-DPS-DMAC and DBTO-DMAC.[24]

As shown in Figure 5, TTR, DBTO and DPS acceptor moieties with different rigidities behave differently in photophysical properties. By virtue of the geometric analysis, we observed that these three acceptor moieties create perfectly orthogonal geometries with DMAC unit. On the other hand, their coupling with PXZ donor group leads to ~10 shift from orthogonality (Table S4). We further investigated their electron accepting abilities with the help of E_g values and observed that LUMO energies decrease in the order of

TXO2-PXZ, p-PXZ-DPS-PXZ and DBTO-PXZ which indicates that DBTO is the strongest and TXO2 is the weakest electron acceptor. On the other hand, ΔE_{ST} values of the six emitters under investigation are extremely small both experimentally and theoretically. This indicates that any possible difference in RISC mechanisms of these compounds can arise from any other parameter, but not from the singlet-triplet energy gap. At this stage, since the natures of triplet states will be the determinative factor in RISC, the effects of these acceptor moieties on the natures of excited triplet states have been analyzed. The results obtained using metahybrid M062X functional are shown in Table 3.

Table 3. Natures of S_1, T_1-T_5 states computed at M062X/6-31+G(d,p) level of theory in toluene (TXO2-PXZ, *p*-PXZ-DPS-PXZ, TXO2-DMAC, *p*-DMAC-DPS-DMAC, DBTO-DMAC) and in dichloromethane (DBTO-PXZ).

Emitters	S_1 (Φs)	T_1 (Φs)	T_2 (Φs)	T_3 (Φs)	T_4 (Φs)	T_5 (Φs)
TXO2-PXZ	CT (0.2809)	LE (0.8393)	LE (0.8372)	CT (0.3879)	CT (0.3939)	LE (0.8082)
p-PXZ-DPS-PXZ	CT (0.2485)	CT-LE (0.4301)	CT-LE (0.3921)	CT-LE (0.7840)	CT-LE (0.7951)	CT-LE (0.7599)
DBTO-PXZ	CT (0.1854)	CT (0.3842)	CT (0.4018)	CT-LE (0.6394)	CT-LE (0.6383)	LE (0.9497)
TXO2-DMAC	CT (0.3465)	CT (0.3422)	CT (0.3206)	LE (0.8951)	LE (0.8951)	LE (0.7484)
p-DMAC-DPS-DMAC	CT (0.1642)	CT (0.1692)	CT (0.1677)	LE (0.8800)	LE (0.8798)	LE (0.7097)
DBTO-DMAC	CT (0.1712)	CT (0.2102)	CT (0.2044)	LE (0.9530)	CT-LE (0.4715)	CT-LE (0.4789)

The S_1 state natures of all emitters were found to be in CT character with perfectly separated FMOs. Their T_1 and T_2 states are generally in CT character except TXO2-PXZ and *para*-PXZ. For T_2, T_3, T_4 and T_5 states, while *para*-PXZ emitter represents mixed character, DBTO-PXZ emitter represents an obvious increase in LE transitions. On the other hand, TXO2-PXZ does not represent any regular trend from T_2 to T_5. $\Delta\Phi_s$ values in Figure 5 are in well agreement with the SOC values which represent an enhancement with the increase nature difference between singlet and triplet states. Comparing with their phenoxazine analogues, we observed the better FMO separation of T_1 and T_2 states, which is reflected in Φ_s values, of DMAC containing emitters (see Table 3). Hence, the SOC from these low lying triplet states exhibit smaller values than their PXZ- analogues. Besides lower Φs indices of the first two triplet states, T_3, T_4 and T_5 states show larger LE character, thus, larger SOC values. Considering all comparisons, we learned that the different acceptor moieties may yield various SOC values with higher triplet levels and there is no a regular trend between these acceptor groups.

Further analyses of excited state energies show that going from TXO2-PXZ to DBTO-PXZ, energies of the first singlet states decrease (see Figure 6), thus, compared to TXO2 acceptor moiety, DPS and DBTO yield bathochromically shifted absorption spectra (see Figure S6). According to the our theoretical findings reported in Figure 6, energy comparisons are in well agreement with the experimental emission spectra of investigated compounds which emit in blue-green, blue and yellow for TXO2-PXZ,[52] p-PXZ-DPS-PXZ[52] and DBTO-PXZ[54] compounds respectively. Moreover, we observed the similar decreasing energy trend for triplet states, and the energies of T_1 and T_2 states are iso-energetic in all emitters. This degeneracy of triplet states leads to state mixing between the states in different nature, thus, leading to larger SOC values and more efficient RISC processes. On the other hand, for compounds with iso-energetic identical nature states, such as, TXO2-DMAC, *p*-DMAC-DPS-DMAC and DBTO-DMAC, hyperfine coupling (HF) can play an important role in enhancing ISC/RISC processes. Hyperfine couplings are mainly observed in compounds, which have identical nature singlet and triplet states leading to very small SOC values.[55] Different from SOC-driven RISC pathway (^{3}LE $\rightarrow$ ^{1}CT), hyperfine coupling induced RISC can be observed between identical nature states (^{3}CT $\rightarrow$ ^{1}CT). Therefore, as an alternative to the SOC-driven RISC mechanism, efficient RISC can also occur simultaneously *via* both the SOC and hyperfine coupling processes.[56]

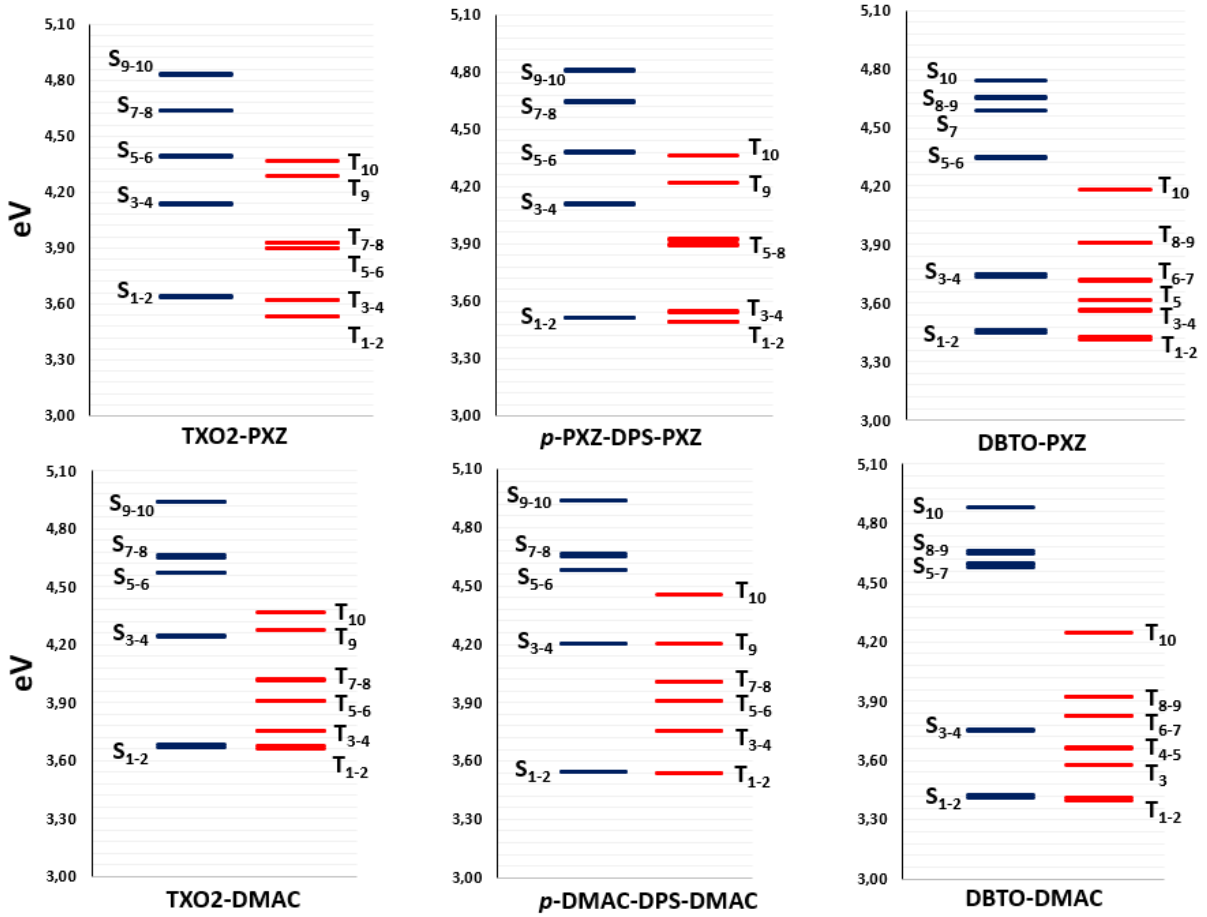

Figure 6. Energy levels of TTR, DPS and DBTO containing TADF emitters computed at M062X/6-31+G(d,p) level of theory in toluene (TXO2-PXZ, *p*-PXZ-DPS-PXZ, TXO2-DMAC, *p*-DMAC-DPS-DMAC, DBTO-DMAC) and in dichloromethane (DBTO-PXZ).

To sum up, the nature of excited states for TXO2, DPS and DBTO acceptor moieties are similar and surprisingly, Φ_S values of emitters with DPS (flexible) and DBTO (rigid) acceptor groups are found to be very close to each other. Additionally, LUMO energies of these emitters are also quite similar representing their similar electron accepting abilities, which is consistent with their similar absorption spectra (see Figure S6). Moreover, energy level alignments of this molecule set was found to behave differently from the first two groups (Figure 4). In contrast to Groups 1 and 2, the molecule set under investigation have low lying iso-energetic singlet and triplet levels with similar nature of states. Thus, contrary to the SOC-driven RISC between different nature of states, we theoretically observe that HF coupling may also play a role in RISC process.

Effects of Phenyl Bridges on Photophysical Properties

Density functional theory calculations of Groups 3 and 4 were performed on ground state energy surfaces. As shown in Figure 7, Group 4 is the bridge-containing analogue of Group 3. Herein, we aimed to theoretically examine the effects of bridging the donor and acceptor moieties with a phenyl ring to observe the change in properties such as, geometric parameters, excited state energies, FMO separations (energy gaps between HOMO and LUMO orbitals) and energy gaps between the excited states involved in the RISC process. In the set of molecules under investigation, the TTR moiety with two sulfur atoms has been selected as the acceptor group and Cz, DMAC, PXZ and PTZ moieties with different steric hindrance and aromaticity have been selected as the donor moieties.

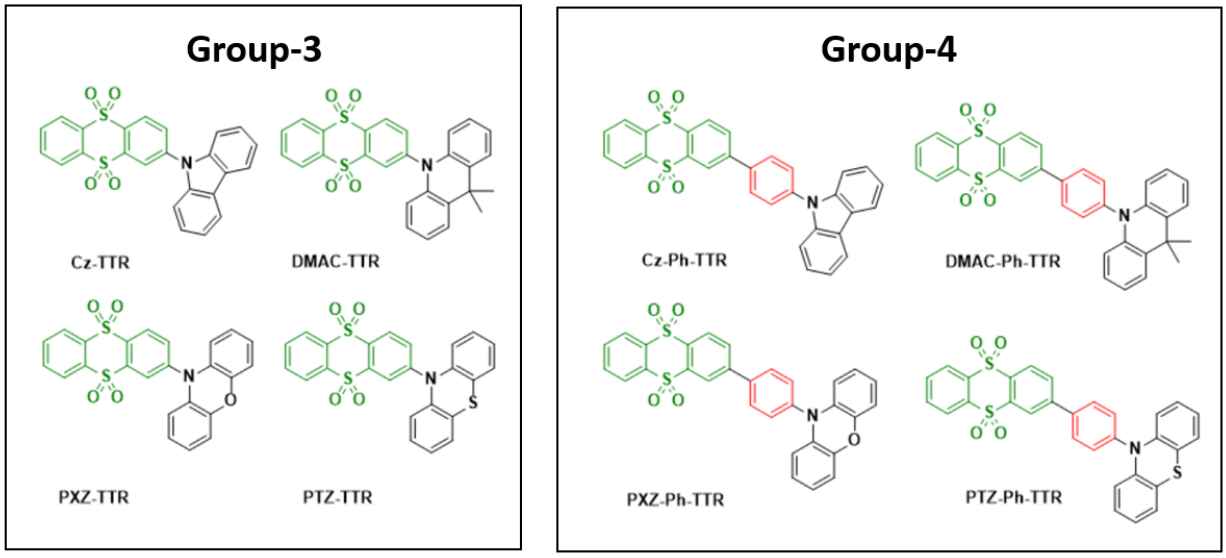

Figure 7. Bridged and non-bridged TADF emitters with TTR acceptor moiety. Compounds: Cz-TTR,[57] DMAC-TTR,[58] PXZ-TTR,[59] PTZ-TTR,[58] Cz-Ph-TTR,[60] DMAC-Ph-TTR,[58] PXZ-Ph-TTR[61] and PTZ-Ph-TTR.[58]

As reported in Table S5 and Table S6, effect of inserting a phenyl bridge largely affected the torsion angles between acceptor groups and their adjacent moieties. As an expection, the carbazole moiety in Cz-TTR and Cz-Ph-TTR exhibits ~40 and ~37 torsion angle, respectively; thus, inserting phenyl bridge in carbazole containing emitter do not cause large effect on torsion angle of Cz moiety. As reported in Table 4, both experimental and theoretical ΔE_{ST} values for the Cz-TTR emitter are smaller than their phenyl containing

analogue (Cz-Ph-TTR), a situation which can be attributed to the larger electron-hole separation (see Phi-S indices in Table 5).

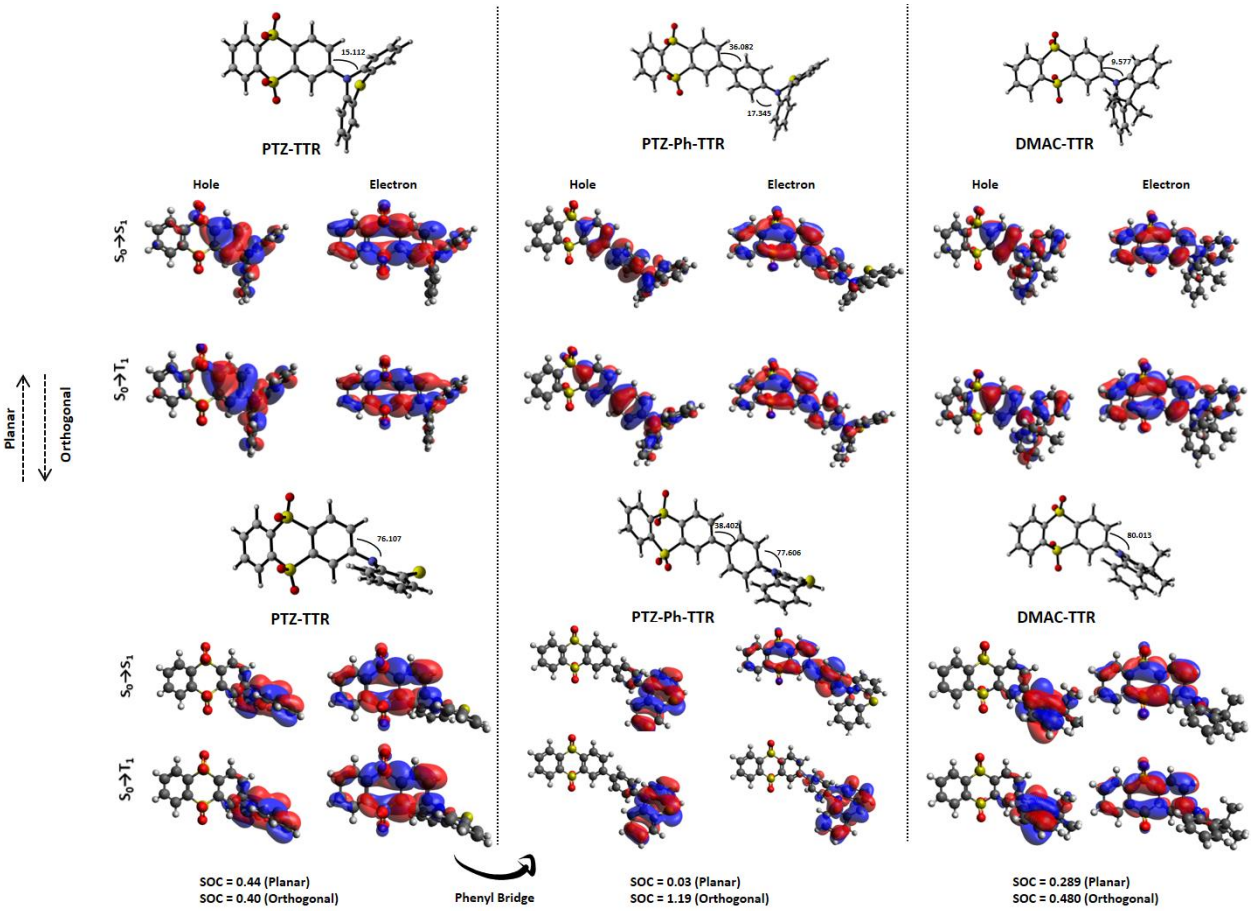

Figure 8.Optimized geometries and electron - hole ornitals of planar and orthogonal conformers of PTZ-TTR, PTZ-Ph-TTR and DMAC-TTR emitters computed at M06-2X/6-31+G(d,p) level of theory.

On the other hand, DMAC and PTZ containing emitters were found to have two possible conformers, which are orthogonal and planar. As shown in Figure 8, relative energy differences between orthogonal and planar conformers of these emitters are very small, indicating the presence of iso-energetic low energy conformers in their D-A and D-π-A structures.

Table 4. HOMO-LUMO energies, E_g and ΔE_{ST} values of Group 4 and 5 emitters computed at M062X/6-31+G(d,p) level of theory in toluene (for Cz-Ph-TTR, DMAC-TTR, DMAC-Ph-TTR, PXZ-TTR, PXZ-Ph-TTR, PTZ-TTR, PTZ-Ph-TTR) and in ethy ethanoate (Cz-TTR).

Emitters	HOMO	LUMO	LUMO - HOMO (E_g) (eV)	ΔE_{ST} a=experiment b=theoretical
Cz-TTR	-0.2659	-0.0666	0.1993	0.10[a] / 0.05[b]
Cz-Ph-TTR	-0.2566	-0.0668	0.1899	0.30 [a] / 0.15 [b]
DMAC-TTR (Planar)	-0.2695	-0.0550	0.2145	0.45[a] / 0.33 [b]
DMAC-TTR (Orthogonal)	-0.2535	-0.0660	0.1875	0.01[a] / -
DMAC-Ph-TTR (only orthogonal)	-0.2393	-0.0669	0.1723	0.06 [a] / 0.00 [b]
PXZ-TTR	-0.2458	-0.0678	0.1780	- / 0.37 [b]
PXZ-Ph-TTR	-0.2390	-0.0677	0.1712	0.05 [a] / 0.02 [b]
PTZ-TTR (Planar)	-0.2722	-0.0546	0.2176	0.38[a] / 0.25 [b]
PTZ-TTR (Orthogonal)	-0.24967	-0.0674	0.1822	0.10[a] / 0.01[b]
PTZ-Ph-TTR (Planar)	-0.2592	-0.0611	0.1981	0.57[a] / 0.20[b]
PTZ-Ph-TTR (Orthogonal)	-0.2431	-0.0676	0.1755	0.01[a] / 0.07[b]

According to Table 4, effects of orthogonal geometries on singlet–triplet energy gap were well reproduced and their TADF activity due to the iso-energetic low energy conformers has been proved once again. Moreover, we also observed that the orthogonal geometries lead to a decrease in the LUMO and an increase in the HOMO energies, thus, they yield smaller E_g values. Due to the smaller E_g values calculated for orthogonal geometries, their emission spectra were expected to be bathochromically shifted compared to their planar analogues, and although we did not calculate theoretical emission spectra, by way of comparing with experimental spectra reported in literature, we concluded that the calculated E_g values are consistent with the experimental data reported in literature.[58]To further study the effects of phenyl insertion and geometry changes on photophysical properties, we computed Phi-S indices at the M062X/6-31+G(d,p) level of theory in experimental solvents.

Table 5. Natures of S_1, T_1-T_5 states computed at M062X/6-31+G(d,p) level of theory in toluene (for Cz-Ph-TTR, DMAC-TTR, DMAC-Ph-TTR, PXZ-TTR, PXZ-Ph-TTR, PTZ-TTR, PTZ-Ph-TTR) and in ethy ethanoate (Cz-TTR).

Emitters	S1 (Φs)	T1 (Φs)	T2 (Φs)	T3 (Φs)	T4 (Φs)	T5 (Φs)
Cz-TTR	CT-LE (0.5372)	LE (0.6815)	LE (0.9669)	LE (0.7556)	LE (0.6962)	LE (0.9489)
Cz-Ph-TTR	CT-LE (0.7649)	LE (0.9017)	LE (0.7723)	LE (0.9601)	LE (0.9118)	LE (0.9495)
DMAC-TTR (Planar)	CT-LE (0.7150	LE (0.7941)	LE (0.7471)	LE (0.9543)	LE (0.9551)	LE (0.9622)
DMAC-TTR (Orthogonal)	CT 0.2008	CT 0.2255	CT 0.4256	LE 0.8829	LE 0.9490	LE 0.7289
DMAC-Ph-TTR (only orthogonal)	CT (0.4644)	CT (0.4545)	LE (0.9450)	LE (0.8793)	LE (0.7088)	LE (0.7127)
PXZ-TTR	CT-LE (0.5143)	CT-LE (0.5045)	CT (0.4417)	LE (0.7709)	CT-LE (0.5976)	CT-LE (0.5589)
PXZ-Ph-TTR	CT (0.2247)	CT-LE (0.5210)	LE (0.7435)	LE (0.9473)	LE (0.8069)	LE (0.7076)
PTZ-TTR (Planar)	LE (0.6951)	LE (0.8187)	LE (0.7689)	LE (0.9175)	LE (0.8723)	LE (0.9630)
PTZ-TTR (Orthogonal)	CT (0.1588)	CT (0.1974)	LE (0.7363)	CT-LE (0.5658)	LE (0.7236)	LE (0.9450)
PTZ-Ph-TTR (Planar)	CT-LE (0.6631)	LE (0.8496)	LE (0.8313)	LE (0.8525)	LE (0.9040)	LE (0.8741)
PTZ-Ph-TTR (Orthogonal)	CT (0.3481)	LE (0.7746)	CT-LE (0.4652)	LE (0.9449)	LE (0.6797)	LE (0.6983)

As summarized in Table 5 and as represented in Figure 9, insertion of phenyl bridge may increase or decrease the electron and hole separation of triplet states differently. Due to better separation in orthogonal geometries, going from planar to orthogonal conformers, a general decrease in Phi-S indices was observed. Since the S_1 states of orthogonal emitters were found to be in CT or mixed character, their SOC values with triplet states in strong LE character were observed to be the strongest couplings (see Figure 8). We further compared the electron – hole overlaps of bridged and non-bridged emitters, and observed that for Cz, PXZ and PTZ containing emitters, significant differences arise from the presence of phenyl bridges.

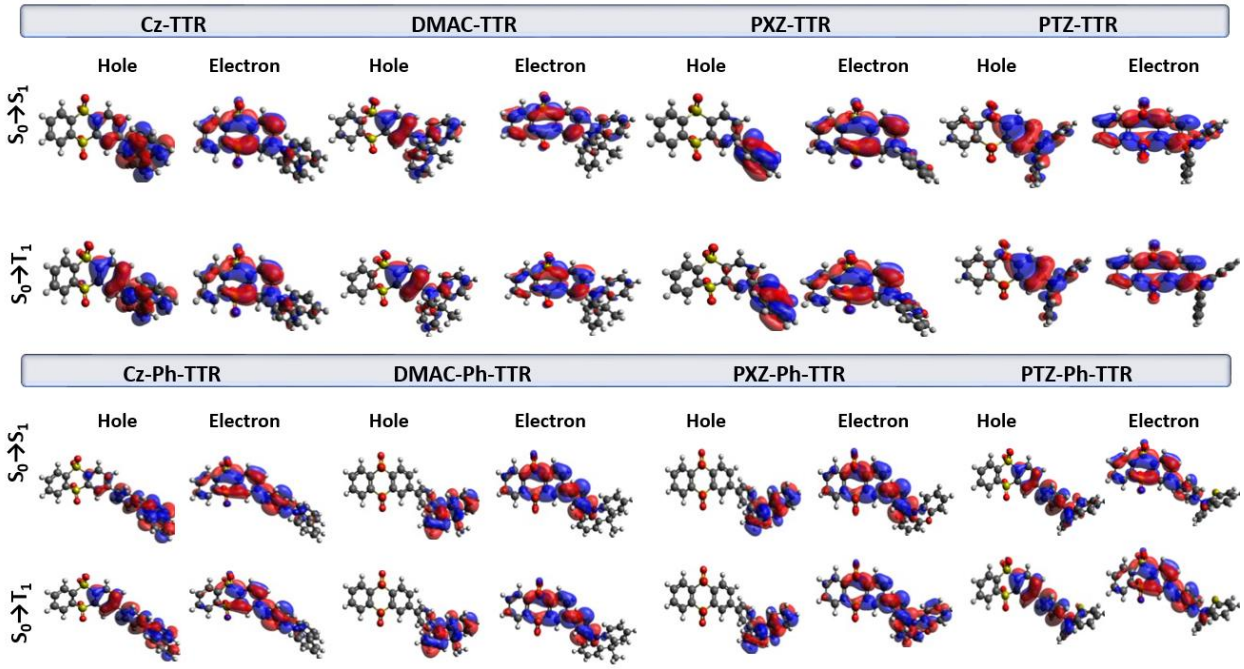

Figure 9. Frontier molecular orbital distributions of Group 4 and Group 5 emitters computed at M06-2X/6-31+G(d,p) level of theory in toluene (for Cz-Ph-TTR, DMAC-TTR, DMAC-Ph-TTR, PXZ-TTR, PXZ-Ph-TTR, PTZ-TTR, PTZ-Ph-TTR) and in ethy ethanoate (Cz-TTR).

However, negative or positive effect of using phenyl bridge can vary in different emitters. For instance, while the insertion of a phenyl bridge to Cz-TTR and PTZ-TTR lead to increase in electron-hole overlap, separation increased in PXZ-Ph-TTR emitter.

The contribution of a phenyl bridge to excited state energies and energy gaps were also examined and the relative positions of the excited singlet and triplet states were reported in Figure 10. With the incorporation of the phenyl moiety, an increasing trend in S_1 energy levels was observed in all emitters, except for DMAC-Ph-TTR. This situation can be attributed to the larger decrease in the torsion angle of DMAC moiety in phenyl containing emitter compared to the other donor moieties which leads to larger increase in planarity and conjugation length, thus decrease in S_1 energy (see Table S5 and S6).

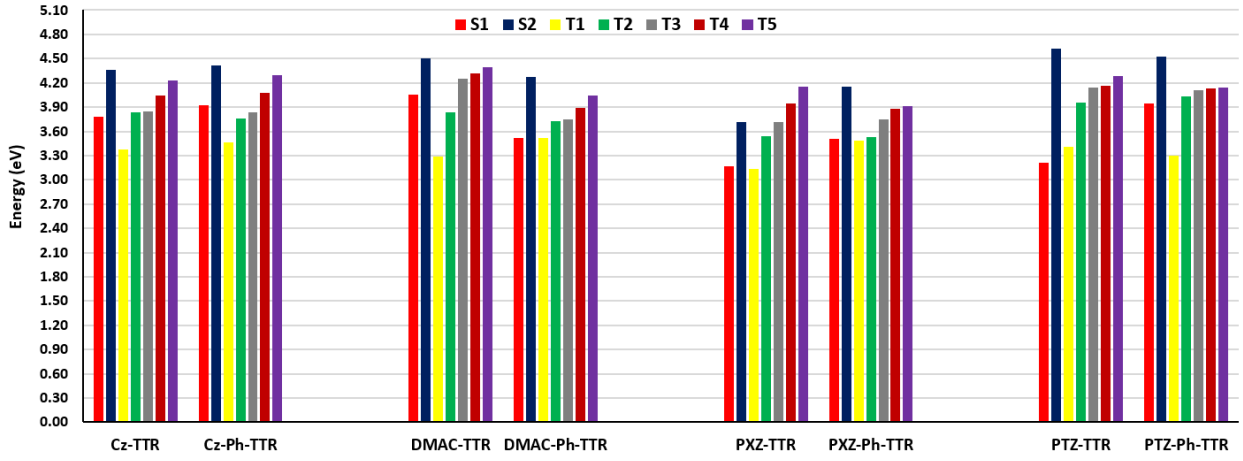

Figure 10. Energies of singlet and triplet excited states computed at M062X/6-31+G(d,p) level of theory in toluene (for Cz-Ph-TTR, DMAC-TTR, DMAC-Ph-TTR, PXZ-TTR, PXZ-Ph-TTR, PTZ-TTR, PTZ-Ph-TTR) and in ethy ethanoate (Cz-TTR).

On the other hand, compared to the D-A emitters, T_1 energies of phenyl containing analogues were increased, except compound with the PTZ moiety. Despite the benefit of longer conjugation in bridge containing D-π-A emitters, increased electron-hole overlap generally led to an increase in the LE character of the T_1 state. Correspondingly, SOC values of phenyl containing emitters were increased, leading to larger RISC probabilities.

Summarizing, insertion of the π-bridge affected the behavior of emitters differently. While some materials exhibit larger ΔE_{ST} values with π-linkers, some of them represented smaller ΔE_{ST} values. On the other hand, HOMO-LUMO gaps of the emitters were found to be very close in emitters with or without π-bridges. Notably, DMAC-TTR and PTZ-TTR emitters were found to have iso-energetic low energy conformers conformers with different photophysical properties. Our findings in ΔE_{ST} and nature of states analyses confirmed the TADF activity of orthogonal conformers. Lastly, in most of the emitters under investigation, phenyl unit containing TADF materials represented larger SOC values.

CONCLUSION

In summary, we present a comprehensive theoretical study on structural and photophysical properties of sulfone-based TADF emitters. Our investigations reveal that the molecule set under investigation presents various geometric behaviors, such as bearing bent conformations which prevent the formation

of intermolecular excimers as well as having iso-energetic low energy conformers, which exhibit TADF or non-TADF activities. Notably, our analyses on the effects of *meta*- and *para*-conjugation showed that the regioisomers possess different photophysical properties. The first two molecule sets were shown to have multiple triplet levels below the S_1 state, which opens alternative ISC/RISC pathways. Moreover, we also presented the possibilities of IC, ISC and RISC processes between the high lying singlet and triplet levels. Additionally, we observed that the larger amount of state mixing in iso-energetic triplet levels below the S_1 state enhances the SOC values and RISC probabilities. Moreover, we observed that for compounds with iso-energetic identical nature states, hyperfine coupling (HF) can play an important role in enhancing ISC/RISC processes.

We further modeled the effects of rigid acceptor moieties in TADF performance and our findings reveal that the hyperfine couplings between the identical nature states may also enhance RISC probabilities. In the last part of our study, we discussed the effects of phenyl bridges on structures and photophysical properties. Our findings show that most of the phenyl bridge containing TADF emitters present larger SOC values. This work is intended to provide insight and pave a way to design new TADF emitters. In light of our findings, it is possible to design new emitters with desired properties and give rise to the developments in TADF technology with new molecule designs.

AUTHOR INFORMATION

Corresponding Author: Saron Catak
E-mail: saron.catak@boun.edu.tr
‡ These authors contributed equally to this study.

ACKNOWLEDGEMENT

This work is supported by the TUBITAK ULAKBIM High Performance and Grid Computing Center (TRUBA resources). SC, PU and AH thank TUBITAK (Project Number: 118Z914) and BAP-M (16863) for financial support.

References

(1) Kesari, S.; Mishra, B. K.; Panda, A. N. Excited States in RED/near Infrared Region TADF Molecules: TDDFT vs ADC(2). *Chem. Phys. Lett.* **2022**, *791* (November 2021), 139383. https://doi.org/10.1016/j.cplett.2022.139383.

(2) Yang, L.; Li, X.; Yang, Q.; Wang, S.; Tian, H.; Ding, J.; Wang, L. Efficient Narrowband Red Electroluminescence from a Thermally Activated Delayed Fluorescence Polymer and Quantum

Dot Hybrid. *Chem. Eng. J.* **2022**, *436* (November 2021), 135221. https://doi.org/10.1016/j.cej.2022.135221.

(3) Chen, Y. W.; Tsai, C. C.; Chih, H. Y.; Tsai, H. Y.; Wang, W. Y.; Liu, G. Y.; Wu, M. Y.; Chang, C. H.; Lu, C. W. Realizing Performance Improvement of Borylated TADF Materials for OLEDs. *Dye. Pigment.* **2022**, *197* (September 2021), 109892. https://doi.org/10.1016/j.dyepig.2021.109892.

(4) Zheng, Y.; Huo, J.; Xiao, S.; Shi, H.; Ma, D.; Tang, B. Z. Synthesis, Photoluminescence and Electroluminescence Properties of a New Blue Emitter Containing Carbazole, Acridine and Diphenyl Sulfone Units. *Org. Electron.* **2022**, *101* (November 2021), 106411. https://doi.org/10.1016/j.orgel.2021.106411.

(5) Mellerup, S. K.; Wang, S. Boron-Doped Molecules for Optoelectronics. *Trends Chem.* **2019**, *1* (1), 77–89. https://doi.org/10.1016/j.trechm.2019.01.003.

(6) Kothavale, S. S.; Lee, J. Y. Three- and Four-Coordinate, Boron-Based, Thermally Activated Delayed Fluorescent Emitters. *Adv. Opt. Mater.* **2020**, *2000922*, 1–24. https://doi.org/10.1002/adom.202000922.

(7) Bas, E. E.; Ulukan, P.; Monari, A.; Aviyente, V.; Catak, S. Photophysical Properties of Benzophenone-Based TADF Emitters in Relation to Their Molecular Structure. *J. Phys. Chem. A* **2022**, *126* (4), 473–484. https://doi.org/10.1021/acs.jpca.1c08320.

(8) Ren, W.; Son, K. R.; Park, T. H.; Murugadoss, V.; Kim, T. G. Manipulation of Blue TADF Top-Emission OLEDs by the First-Order Optical Cavity Design: Toward a Highly Pure Blue Emission and Balanced Charge Transport. *Photonics Res.* **2021**, *9* (8), 1502. https://doi.org/10.1364/prj.432042.

(9) Rajamalli, P.; Rizzi, F.; Li, W.; Jinks, M. A.; Gupta, A. K.; Laidlaw, B. A.; Samuel, I. D. W.; Penfold, T. J.; Goldup, S. M.; Zysman-Colman, E. Using the Mechanical Bond to Tune the Performance of a Thermally Activated Delayed Fluorescence Emitter**. *Angew. Chemie - Int. Ed.* **2021**, *60* (21), 12066–12073. https://doi.org/10.1002/anie.202101870.

(10) Smith, P. O.; Black, D. J.; Pal, R.; Avó, J.; Dias, F. B.; Linthwaite, V. L.; Cann, M. J.; Pålsson, L. O. Applying TADF Emitters in Bioimaging and Sensing—A Novel Approach Using Liposomes for Encapsulation and Cellular Uptake. *Front. Chem.* **2021**, *9*. https://doi.org/10.3389/fchem.2021.743928.

(11) Hosokai, T.; Nakanotani, H.; Santou, S.; Noda, H.; Nakayama, Y.; Adachi, C. TADF Activation by Solvent Freezing: The Role of Nonradiative Triplet Decay and Spin-Orbit Coupling in Carbazole Benzonitrile Derivatives. *Synth. Met.* **2019**, *252*, 62–68. https://doi.org/10.1016/j.synthmet.2019.04.005.

(12) Kim, J. H.; Yun, J. H.; Lee, J. Y. Recent Progress of Highly Efficient Red and Near-Infrared Thermally Activated Delayed Fluorescent Emitters. *Advanced Optical Materials*. Wiley-VCH Verlag September 18, 2018. https://doi.org/10.1002/adom.201800255.

(13) Li, S.; Jin, X.; Yu, Z.; Xiao, X.; Geng, H.; Liao, Q.; Liao, Y.; Wu, Y.; Hu, W.; Fu, H. Design of Thermally Activated Delayed Fluorescent Emitters for Organic Solid-State Microlasers. *J. Mater. Chem. C* **2021**, *9* (23), 7400–7406. https://doi.org/10.1039/d0tc05562j.

(14) Li, W.; Li, M.; Li, W.; Xu, Z.; Gan, L.; Liu, K.; Zheng, N.; Ning, C.; Chen, D.; Wu, Y. C.; Su, S. J. Spiral Donor Design Strategy for Blue Thermally Activated Delayed Fluorescence Emitters. *ACS Appl. Mater. Interfaces* **2021**, *13* (4), 5302–5311. https://doi.org/10.1021/acsami.0c19302.

(15) Traskovskis, K.; Sebris, A.; Novosjolova, I.; Turks, M.; Guzauskas, M.; Volyniuk, D.; Bezvikonnyi, O.; Grazulevicius, J. V.; Mishnev, A.; Grzibovskis, R.; Vembris, A. All-Organic Fast Intersystem Crossing Assisted Exciplexes Exhibiting Sub-Microsecond Thermally Activated Delayed Fluorescence. *J. Mater. Chem. C* **2021**, *9* (13), 4532–4543. https://doi.org/10.1039/d0tc05099g.

(16) Xu, S.; Yang, Q.; Wan, Y.; Chen, R.; Wang, S.; Si, Y.; Yang, B.; Liu, D.; Zheng, C.; Huang, W. Predicting Intersystem Crossing Efficiencies of Organic Molecules for Efficient Thermally Activated Delayed Fluorescence. *J. Mater. Chem. C* **2019**, *7* (31), 9523–9530.

https://doi.org/10.1039/c9tc03152a.
(17) Tu, Z.; Han, G.; Hu, T.; Duan, R.; Yi, Y. Nature of the Lowest Singlet and Triplet Excited States of Organic Thermally Activated Delayed Fluorescence Emitters: A Self-Consistent Quantum Mechanics/Embedded Charge Study. *Chem. Mater.* **2019**, *31* (17), 6665–6671. https://doi.org/10.1021/acs.chemmater.9b00824.
(18) Shi, Y. H.; Wang, F.; Sun, G. Y.; Xie, Y. Z. The Effect of Heavy Atoms Replacement Sites on the Luminescent Ways of D-A-D Type Diphenyl Sulfone Molecules: Thermally Activated Delayed Fluorescence and Phosphorescence. *Spectrochim. Acta - Part A Mol. Biomol. Spectrosc.* **2022**, *264*, 120249. https://doi.org/10.1016/j.saa.2021.120249.
(19) Ren, H.; Song, Y.; Yu, R.; Tian, M.; He, L. Through-Space Charge-Transfer Emitters Featuring High Radiative Decay Rates for Efficient Organic Light-Emitting Diodes. *Dye. Pigment.* **2022**, *204* (April), 110389. https://doi.org/10.1016/j.dyepig.2022.110389.
(20) Kim, I.; Jeon, S. O.; Jeong, D.; Choi, H.; Son, W. J.; Kim, D.; Rhee, Y. M.; Lee, H. S. Spin-Vibronic Model for Quantitative Prediction of Reverse Intersystem Crossing Rate in Thermally Activated Delayed Fluorescence Systems. *J. Chem. Theory Comput.* **2020**, *16* (1), 621–632. https://doi.org/10.1021/acs.jctc.9b01014.
(21) Leng, C.; You, S.; Si, Y.; Qin, H. M.; Liu, J.; Huang, W. Q.; Li, K. Unraveling the Mechanism of Near-Infrared Thermally Activated Delayed Fluorescence of TPA-Based Molecules: Effect of Hydrogen Bond Steric Hindrance. *J. Phys. Chem. A* **2021**, *125* (14), 2905–2912. https://doi.org/10.1021/acs.jpca.1c00739.
(22) Yang, S. Y.; Wang, Y. K.; Peng, C. C.; Wu, Z. G.; Yuan, S.; Yu, Y. J.; Li, H.; Wang, T. T.; Li, H. C.; Zheng, Y. X.; Jiang, Z. Q.; Liao, L. S. Circularly Polarized Thermally Activated Delayed Fluorescence Emitters in Through-Space Charge Transfer on Asymmetric Spiro Skeletons. *J. Am. Chem. Soc.* **2020**, *142* (41), 17756–17765. https://doi.org/10.1021/jacs.0c08980.
(23) Ulukan, P.; Bas, E. E.; Ozek, R. B.; Dal Kaynak, C.; Monari, A.; Aviyente, V.; Catak, S. Computational Descriptor Analysis on Excited State Behaviours of a Series of TADF and Non-TADF Compounds. *Phys. Chem. Chem. Phys.* **2022**, *24* (26), 16167–16182. https://doi.org/10.1039/d2cp01323a.
(24) Kukhta, N. A.; Batsanov, A. S.; Bryce, M. R.; Monkman, A. P. Importance of Chromophore Rigidity on the Efficiency of Blue Thermally Activated Delayed Fluorescence Emitters. *J. Phys. Chem. C* **2018**, *122* (50), 28564–28575. https://doi.org/10.1021/acs.jpcc.8b10867.
(25) Hussain, A.; Yuan, H.; Li, W.; Zhang, J. Theoretical Investigations of the Realization of Sky-Blue to Blue TADF Materials: Via CH/N and H/CN Substitution at the Diphenylsulphone Acceptor. *J. Mater. Chem. C* **2019**, *7* (22), 6685–6691. https://doi.org/10.1039/c9tc01449g.
(26) Frisch, M. J.; Trucks, G. W.; Schlegel, H. B.; Scuseria, G. E.; Robb, M. A.; Cheeseman, J. R.; Scalmani, G.; Barone, V.; Petersson, G. A.; Nakatsuji, H.; Li, X.; Caricato, M.; Marenich, A. V.; Bloino, J.; Janesko, B. G.; Gomperts, R.; Mennucci, B.; Hratch, I. Gaussian 16, Revision C.01.
(27) te Velde, G.; Bickelhaupt, F. M.; Baerends, E. J.; Fonseca Guerra, C.; van Gisbergen, S. J. A.; Snijders, J. G.; Ziegler, T. Chemistry with ADF. *J. Comput. Chem.* **2001**, *22* (9), 931–967. https://doi.org/10.1002/jcc.1056.
(28) Y. Zhao and D. G. Truhlar. The M06 Suite of Density Functionals for Main Group Thermochemistry, Thermochemical Kinetics, Noncovalent Interactions, Excited States, and Transition Elements: Two New Functionals and Systematic Testing of Four M06-Class Functionals and 12 Other Function. *Theor. Chem. Acc.* **2008**, *120*, 215–241.
(29) R. Ditchfield, W. J. Hehre, and J. A. P. Self-Consistent Molecular Orbital Methods. 9. Extended Gaussian-Type Basis for Molecular-Orbital Studies of Organic Molecules. *J. Chem. Phys.* **1971**, *54*, 724.
(30) Mewes, J. M. Modeling TADF in Organic Emitters Requires a Careful Consideration of the Environment and Going beyond the Franck-Condon Approximation. *Phys. Chem. Chem. Phys.*

2018, *20* (18), 12454–12469. https://doi.org/10.1039/c8cp01792a.
(31) J.-D. Chai and M. Head-Gordon. Long-Range Corrected Hybrid Density Functionals with Damped Atom-Atom Dispersion Corrections. *Phys. Chem. Chem. Phys.* **2008**, *10*, 6615–6620.
(32) Peach, M. J. G.; Williamson, M. J.; Tozer, D. J. Influence of Triplet Instabilities in TDDFT. *J. Chem. Theory Comput.* **2011**, *7* (11), 3578–3585. https://doi.org/10.1021/ct200651r.
(33) L. A. Curtiss, M. P. McGrath, J.-P. Blaudeau, N. E. Davis, R. C. Binning Jr., and L. R. Extension of Gaussian-2 Theory to Molecules Containing Third-Row Atoms Ga-Kr. *J. Chem. Phys.* **1995**, *103*, 6104–6113.
(34) Etienne, T.; Assfeld, X.; Monari, A. New Insight into the Topology of Excited States through Detachment/Attachment Density Matrices-Based Centroids of Charge. *J. Chem. Theory Comput.* **2014**, *10* (9), 3906–3914. https://doi.org/10.1021/ct500400s.
(35) Hanwell, M. D.; Curtis, D. E.; Lonie, D. C.; Vandermeerschd, T.; Zurek, E.; Hutchison, G. R. Avogadro: An Advanced Semantic Chemical Editor, Visualization, and Analysis Platform. *J. Cheminform.* **2012**, *4* (8). https://doi.org/10.1186/1758-2946-4-17.
(36) Van Lenthe, E.; Baerends, E. J. Optimized Slater-Type Basis Sets for the Elements 1-118. *J. Comput. Chem.* **2003**, *24* (9), 1142–1156. https://doi.org/10.1002/jcc.10255.
(37) Dahl, J. P.; Springborg, M. The Morse Oscillator in Position Space, Momentum Space, and Phase Space. *J. Chem. Phys.* **1988**, *88* (7), 4535–4547. https://doi.org/10.1063/1.453761.
(38) A. D. Becke. Density-Functional Thermochemistry. III. The Role of Exact Exchange. *J. Chem. Phys.* **1993**, *98*, 5648–5652.
(39) C. Adamo and V. Barone. Toward Reliable Density Functional Methods without Adjustable Parameters: The PBE0 Model. *J. Chem. Phys.* **1999**, *110*, 6158–6169.
(40) Olivier, Y.; Moral, M.; Muccioli, L.; Sancho-García, J. C. Dynamic Nature of Excited States of Donor-Acceptor TADF Materials for OLEDs: How Theory Can Reveal Structure-Property Relationships. *J. Mater. Chem. C* **2017**, *5* (23), 5718–5729. https://doi.org/10.1039/c6tc05075a.
(41) Kim, C. A.; Van Voorhis, T. Maximizing TADF via Conformational Optimization. *J. Phys. Chem. A* **2021**, *125* (35), 7644–7654. https://doi.org/10.1021/acs.jpca.1c05104.
(42) Tomasi, J.; Mennucci, B.; Cancès, E. The IEF Version of the PCM Solvation Method: An Overview of a New Method Addressed to Study Molecular Solutes at the QM Ab Initio Level. *J. Mol. Struct. THEOCHEM* **1999**, *464* (1–3), 211–226. https://doi.org/10.1016/S0166-1280(98)00553-3.
(43) Legault, C. Y. CYLview Visualization and Analysis Software for Computational Chemistry 1.0b.
(44) Bezvikonnyi, O.; Gudeika, D.; Volyniuk, D.; Mimaite, V.; Sebastine, B. R.; Grazulevicius, J. V. Effect of Donor Substituents on Thermally Activated Delayed Fluorescence of Diphenylsulfone Derivatives. *J. Lumin.* **2019**, *206* (October 2018), 250–259. https://doi.org/10.1016/j.jlumin.2018.10.018.
(45) Xie, Z.; Chen, C.; Xu, S.; Li, J.; Zhang, Y.; Liu, S.; Xu, J.; Chi, Z. White-Light Emission Strategy of a Single Organic Compound with Aggregation-Induced Emission and Delayed Fluorescence Properties. *Angew. Chemie - Int. Ed.* **2015**, *54* (24), 7181–7184. https://doi.org/10.1002/anie.201502180.
(46) Lee, I. H.; Song, W.; Lee, J. Y. Aggregation-Induced Emission Type Thermally Activated Delayed Fluorescent Materials for High Efficiency in Non-Doped Organic Light-Emitting Diodes. *Org. Electron.* **2016**, *29*, 22–26. https://doi.org/10.1016/j.orgel.2015.11.019.
(47) Li, G.; Zhan, F.; Lou, W.; Wang, D.; Deng, C.; Cao, L.; Yang, Y.; Zhang, Q.; She, Y. Efficient Deep-Blue Organic Light-Emitting Diodes Employing Difluoroboron-Enabled Thermally Activated Delayed Fluorescence Emitters. *J. Mater. Chem. C* **2020**, *8* (48), 17464–17473. https://doi.org/10.1039/d0tc04162a.
(48) Zhang, Q.; Li, J.; Shizu, K.; Huang, S.; Hirata, S.; Miyazaki, H.; Adachi, C. Design of Efficient Thermally Activated Delayed Fluorescence Materials for Pure Blue Organic Light Emitting Diodes.

J. Am. Chem. Soc. **2012**, *134* (36), 14706–14709. https://doi.org/10.1021/ja306538w.
(49) Haykir, G.; Aydemir, M.; Danos, A.; Gumus, S.; Hizal, G.; Monkman, A. P.; Turksoy, F. Effects of Asymmetric Acceptor and Donor Positioning in Deep Blue Pyridyl-Sulfonyl Based TADF Emitters. *Dye. Pigment.* **2021**, *194* (June), 109579. https://doi.org/10.1016/j.dyepig.2021.109579.
(50) Li, P.; Cui, Y.; Song, C.; Zhang, H. A Systematic Study of Phenoxazine-Based Organic Sensitizers for Solar Cells. *Dye. Pigment.* **2017**, *137*, 12–23. https://doi.org/10.1016/j.dyepig.2016.09.060.
(51) Pramanik, S. K.; Suja, F. B.; Zain, S.; Pramanik, B. K. Jo Ur Na l P Re. *Bioresour. Technol. Reports* **2019**, 100310.
(52) Pereira, D. D. S.; Dos Santos, P. L.; Ward, J. S.; Data, P.; Okazaki, M.; Takeda, Y.; Minakata, S.; Bryce, M. R.; Monkman, A. P. An Optical and Electrical Study of Full Thermally Activated Delayed Fluorescent White Organic Light-Emitting Diodes. *Sci. Rep.* **2017**, *7* (1), 1–8. https://doi.org/10.1038/s41598-017-06568-3.
(53) Wang, C.; Deng, C.; Wang, D.; Zhang, Q. Prediction of Intramolecular Charge-Transfer Excitation for Thermally Activated Delayed Fluorescence Molecules from a Descriptor-Tuned Density Functional. *J. Phys. Chem. C* **2018**, *122* (14), 7816–7823. https://doi.org/10.1021/acs.jpcc.7b10560.
(54) Cai, X.; Gao, B.; Li, X.; Su, S.-J. 3.2: Singlet-Triplet Splitting Energy Management via Acceptor Substitution: Complanation Molecular Design for Deep-Blue Thermally Activated Delayed Fluorescent Organic Light-Emitting Diodes. *SID Symp. Dig. Tech. Pap.* **2018**, *49*, 16–21. https://doi.org/10.1002/sdtp.12627.
(55) Ogiwara, T.; Wakikawa, Y.; Ikoma, T. Mechanism of Intersystem Crossing of Thermally Activated Delayed Fluorescence Molecules. *J. Phys. Chem. A* **2015**, *119* (14), 3415–3418. https://doi.org/10.1021/acs.jpca.5b02253.
(56) Monkman, A. Photophysics of Thermally Activated Delayed Fluorescence. *Highly Effic. OLEDs Mater. Based Therm. Act. Delayed Fluoresc.* **2018**, 425–463. https://doi.org/10.1002/9783527691722.ch12.
(57) Wang, K.; Liu, W.; Zheng, C. J.; Shi, Y. Z.; Liang, K.; Zhang, M.; Ou, X. M.; Zhang, X. H. A Comparative Study of Carbazole-Based Thermally Activated Delayed Fluorescence Emitters with Different Steric Hindrance. *J. Mater. Chem. C* **2017**, *5* (19), 4797–4803. https://doi.org/10.1039/c7tc00681k.
(58) Wang, K.; Shi, Y. Z.; Zheng, C. J.; Liu, W.; Liang, K.; Li, X.; Zhang, M.; Lin, H.; Tao, S. L.; Lee, C. S.; Ou, X. M.; Zhang, X. H. Control of Dual Conformations: Developing Thermally Activated Delayed Fluorescence Emitters for Highly Efficient Single-Emitter White Organic Light-Emitting Diodes. *ACS Appl. Mater. Interfaces* **2018**, *10* (37), 31515–31525. https://doi.org/10.1021/acsami.8b08083.
(59) Wang, K.; Zheng, C. J.; Liu, W.; Liang, K.; Shi, Y. Z.; Tao, S. L.; Lee, C. S.; Ou, X. M.; Zhang, X. H. Avoiding Energy Loss on TADF Emitters: Controlling the Dual Conformations of D–A Structure Molecules Based on the Pseudoplanar Segments. *Adv. Mater.* **2017**, *29* (47), 1–9. https://doi.org/10.1002/adma.201701476.
(60) Sun, K.; Sun, Y.; Jiang, W.; Huang, S.; Tian, W.; Sun, Y. Highly Efficient and Color Tunable Thermally Activated Delayed Fluorescent Emitters and Their Applications for the Solution-Processed OLEDs. *Dye. Pigment.* **2017**, *139*, 326–333. https://doi.org/10.1016/j.dyepig.2016.12.037.
(61) Xie, G.; Li, X.; Chen, D.; Wang, Z.; Cai, X.; Chen, D.; Li, Y.; Liu, K.; Cao, Y.; Su, S. J. Evaporation- and Solution-Process-Feasible Highly Efficient Thianthrene-9,9′,10,10′-Tetraoxide-Based Thermally Activated Delayed Fluorescence Emitters with Reduced Efficiency Roll-Off. *Adv. Mater.* **2016**, *28* (1), 181–187. https://doi.org/10.1002/adma.201503225.